

Synergistic delay and strength tuning for logical operations in a chaotic neuron

Ying Xu(徐莹)

Citation: Chin. Phys. B, 2026, 35 (**6**): 060201. DOI: 10.1088/1674-1056/ae5786
http://cpb.iphy.ac.cn; http://iopscience.iop.org/cpb

What follows is a list of articles you may be interested in

Sliding-mode-based preassigned-time control of a class of memristor chaotic systems

Jinrong Fan(樊金荣), Qiang Lai(赖强), Qiming Wang(汪其铭), and Leimin Wang(王雷敏)
Chin. Phys. B, 2024, 33 (**11**): 110205. DOI: 10.1088/1674-1056/ad7e9d

Event-based nonfragile state estimation for memristive recurrent neural networks with stochastic cyber-attacks and sensor saturations

Xiao-Guang Shao(邵晓光), Jie Zhang(张捷), and Yan-Juan Lu(鲁延娟)
Chin. Phys. B, 2024, 33 (**7**): 070203. DOI: 10.1088/1674-1056/ad3dcb

Mechanism analysis of regulating Turing instability and Hopf bifurcation of malware propagation in mobile wireless sensor networks

Xi-Xi Huang(黄习习), Min Xiao(肖敏), Leszek Rutkowski, Hai-Bo Bao(包海波), Xia Huang(黄霞), and Jin-De Cao(曹进德)
Chin. Phys. B, 2024, 33 (**6**): 060202. DOI: 10.1088/1674-1056/ad24d5

An improved ISR-WV rumor propagation model based on multichannels with time delay and pulse vaccination

Yafang Dong(董雅芳), Liangán Huo(霍良安), Xiaoxiao Xie(谢笑笑), and Ming Li(李明)
Chin. Phys. B, 2023, 32 (**7**): 070205. DOI: 10.1088/1674-1056/acd2be

A mathematical analysis: From memristor to fracmemristor

Wu-Yang Zhu(朱伍洋), Yi-Fei Pu(蒲亦非), Bo Liu(刘博), Bo Yu(余波), and Ji-Liu Zhou(周激流)
Chin. Phys. B, 2022, 31 (**6**): 060204. DOI: 10.1088/1674-1056/ac615c

---

SPECIAL TOPIC — Biophysical circuits: Modeling & applications in neuroscience

Synergistic delay and strength tuning for logical operations in a chaotic neuron

Ying Xu(徐莹)[†]

School of Mathematics and Statistics, Shandong Normal University, Ji'nan 250014, *China*

(Received 4 February 2026; revised manuscript received 19 March 2026; accepted manuscript online 26 March 2026)

An improved FitzHugh–Nagumo neuron model is proposed, incorporating electromagnetic induction via a flux-controlled memristor and dual autaptic feedback with tunable strengths and delays. This brain-inspired unit can reliably perform AND and OR logic operations under chaotic driving, serving as a tunable nonlinear computing element. Systematic numerical analysis reveals that the synergistic interplay between autaptic delays and strengths plays a key role in achieving optimal logical stochastic resonance. Specifically, the system achieves near-perfect success rates within specific parameter regions, where a compensatory effect enables delay asymmetry to balance synaptic strength mismatch. Furthermore, at lower coupling strengths, a multiple logical resonance phenomenon is observed, in which the success probability exhibits multiple peaks as a function of synaptic delay. This work not only elucidates the dynamical mechanism underlying reliable neuronal logic operation but also provides a co-design principle for tuning neuromorphic circuits, with potential implications for low-power, high-flexibility computing hardware.

Keywords: FitzHugh–Nagumo neuron model, memristor, multi-scale autapse, logical resonance, time delay

PACS: 02.30.Hq, 02.30.Oz, 05.45.–a, 05.40.Ca

DOI: 10.1088/1674-1056/ae5786 **CSTR:** 32038.14.CPB.ae5786

1. Introduction

With the rapid development of neuromorphic computing, the construction of brain-like computing systems that integrate low power consumption and high robustness has become an important research direction at the intersection of information science and neural engineering.[1] Spiking neural networks are inspired by the structure and mechanisms of biological neural systems.[2] Their operation is event-driven, and they also exhibit asynchronous parallelism and utilize spatiotemporal information encoding.[3–5] These characteristics allow spiking neural networks to demonstrate significant potential in energy efficiency and cognitive modeling, making them particularly suitable for edge computing and embedded intelligence scenarios. However, such networks still face the critical challenge of achieving continuous and reliable information processing in unpredictable and noisy environments.[6] To address this challenge, enhancing the information processing capability of individual neurons has emerged as a key breakthrough. In particular, enabling neurons to dynamically and reconfigurably implement basic logic gate functions while maintaining robust responses to noise has become a crucial step toward advancing neuromorphic computing into practical applications.[7–9] This progression also imposes higher demands on the design and implementation of next-generation intelligent hardware. Although biological neurons naturally process information in an analog manner, the introduction of a logical framework enables the investigation of whether nonlinear neural dynamics can be utilized to implement reliable Boolean operations. This approach establishes a connection between the analog information processing of neurons and digital computation, thereby paving the way for the development of reconfigurable and energy-efficient neuromorphic hardware.

The FitzHugh–Nagumo (FHN) neuron model, serving as a simplified version of the Hodgkin–Huxley model, is a classic framework for studying nonlinear dynamics in neurons.[10–12] Previous studies have demonstrated that introducing noise or time delays can enhance neuronal signal processing under specific conditions,[13–15] even enabling logical operations, a phenomenon known as logical resonance.[16–18] However, such approaches predominantly rely on the regulation of external stimuli, thereby exhibiting limited robustness and flexibility. Recent biological studies have identified the autaptic structure as a novel solution to this challenge.[19–21] Autapses are unique self-connecting synaptic structures formed by neurons onto themselves and are widely present across various brain regions.[22–24] They provide a multi-scale self-feedback regulatory mechanism, enabling neurons to modulate their own activity across different time scales.[25] Consequently, this structure significantly enhances both information processing capacity and functional diversity.

In recent years, the rapid development of neuromorphic computing has made the construction of brain-like computing systems that combine biological plausibility, low power con-

[†]Corresponding author. E-mail: uryysunshine@163.com

© 2026 Chinese Physical Society and IOP Publishing Ltd. All rights, including for text and data mining, AI training, and similar technologies, are reserved.

sumption, and high robustness an important research direction in the field of artificial intelligence.[26] This trend is primarily driven by the fundamental challenges faced by traditional computing architectures in processing real-time perception–motion control tasks.[27–30] For example, in systems requiring high-precision control, such as bionic robotic arms, high energy consumption and computational delays often occur, making it difficult to meet the demands of real-time decision-making in dynamic environments.[31–36] These limitations become particularly prominent in complex tasks such as multi-degree-of-freedom cooperative control, online trajectory planning, and perception of the external environment. Specifically, such functional neurons can be embedded into the joint control modules of robotic arms to process multi-modal sensory information, such as visual and tactile inputs, and generate smooth and precise motor commands.[37–40] Compared to conventional control methods, this bio-inspired strategy not only significantly reduces the energy consumption of the system but also improves response speed and control accuracy, enabling better adaptation to dynamically changing operational environments.[41–44] Based on this, this paper introduces a multi-scale autaptic structure, which consists of two self-feedback loops with independently tunable strengths and delays, to systematically investigate its regulatory mechanism on the computational characteristics of the improved FHN neuron model. Through numerical simulations and nonlinear dynamical analysis, we found that the multi-scale autapse can induce multiple logical resonance phenomena. This mechanism enables a single neuron to efficiently perform fundamental logic operations such as AND and OR, significantly enhancing the functional robustness and adaptability of the system in noisy environments. More importantly, this multi-scale feedback provides a new implementation pathway for constructing functional neurons.

2. Model and scheme

Let us consider a single neuron driven by two autaptic signals with arbitrary differences in both strength and delay time. The dynamics of the neuron are described using the FHN model,[45] and the specific model setup is as follows:

$$\begin{cases} \varepsilon \dfrac{\mathrm{d}x}{\mathrm{d}t} = x - \dfrac{x^3}{3} - y, \\ \dfrac{\mathrm{d}y}{\mathrm{d}t} = x + a + I. \end{cases} \tag{1}$$

Here, the timescale parameter ε, typically set to a value much smaller than 1, governs the difference in rates of change between the fast variable x and the slow variable y. A smaller value of ε indicates faster variation in x and more pronounced relaxation oscillation characteristics. The parameter a primarily influences the position of the y-nullcline, thereby modulating the excitation threshold and resting potential of the system; even slight modifications can significantly alter the dynamical stability. When the parameter $a > 1$, the system exhibits excitable characteristics, whereas when $a < 1$, it demonstrates oscillatory behavior. In this study, the parameter for the AND logic gate is set to $a = 1.05$, while the OR logic gate adopts a configuration of $a = 1$. The external current I is introduced into the recovery variable y rather than the membrane potential x because y governs the slow dynamics and is more sensitive to external modulation. This design better mimics synaptic input affecting the neuron's recovery process. The total input is given by

$$I = (s_1(t) + s_2(t))\, Du(t), \tag{2}$$

where $s_1(t)$ and $s_2(t)$ are binary logic inputs, and $u(t)$ is a chaotic signal generated by the Lorenz system,[46] defined as:

$$\begin{cases} \dfrac{\mathrm{d}u}{\mathrm{d}t} = \sigma(v - u), \\ \dfrac{\mathrm{d}v}{\mathrm{d}t} = u(\rho - w) - v, \\ \dfrac{\mathrm{d}w}{\mathrm{d}t} = uv - \mu w. \end{cases} \tag{3}$$

The parameters are set as $\sigma = 10$, $\rho = 28$, and $\mu = 8/3$. Using this parameter set, a specific chaotic state is induced in the system, and the generated chaotic signal is used as the primary driver for the rest of the model. To more accurately simulate the electromagnetic field effects induced by the time-varying distribution of intracellular and extracellular ion concentrations, a magnetic flux variable is introduced to characterize the electromagnetic induction phenomena excited by the membrane current. Furthermore, constitutive coupling between the membrane potential and magnetic flux is achieved through the physical properties of the memristor. Memristors are primarily categorized into flux-controlled and charge-controlled types. This work employs the flux-controlled type, modeled as follows:

$$\rho(\phi) = \frac{\mathrm{d}q(\phi)}{\mathrm{d}\phi} = \alpha + 3\beta\phi^2. \tag{4}$$

Here, $q(\phi)$ denotes the memductive charge, while α and β represent characteristic parameters of the memristor. Taking into account the electromagnetic induction effect, the dynamics of the three-variable FitzHugh–Nagumo model with dual autaptic stimuli are described by the following equations:

$$\begin{cases} \varepsilon \dfrac{\mathrm{d}x}{\mathrm{d}t} = x - \dfrac{x^3}{3} - y - k_0\rho(\phi)x + I_{\mathrm{syn1}} + I_{\mathrm{syn2}}, \\ \dfrac{\mathrm{d}y}{\mathrm{d}t} = x + a + I, \\ \dfrac{\mathrm{d}\phi}{\mathrm{d}t} = k_1 x - k_2\phi. \end{cases} \tag{5}$$

Here, the third variable ϕ represents the magnetic flux, and $\rho(\phi)$ denotes the memductance. The gain parameters k_0, k_1,

and k_2 collectively regulate the strength of the electromagnetic induction effect, while the term $k_0\rho(\phi)x$ describes the magnetic flux-dependent modification of the membrane potential, corresponding to the generation of an induced current. The dual autaptic stimuli are directly fed back to the membrane potential x, simulating the modulation of rapid electrical activity by local postsynaptic currents. Their mathematical representation is given as follows:[47]

$$I_{\mathrm{syn}i}(t) = -\frac{I_{\mathrm{ch}i}\left(x(t)-V_{\mathrm{syn}i}\right)}{1+\exp\left(-\sigma_i\left(x(t-\tau_i)-\theta_i\right)\right)},$$
$$i = 1,2. \tag{6}$$

The parameter $I_{\mathrm{ch}i}$ denotes the synaptic strength, $V_{\mathrm{syn}i}$ represents the reversal potential, σ_i is the slope factor, θ_i denotes the threshold potential, and τ_i indicates the synaptic delay time. The input signals s_1 and s_2 within the external current I are two independent aperiodic binary square waves, each encoding a distinct logical input according to the following scheme. A logical input of 1 corresponds to an amplitude of 0.3, while a logical input of 0 corresponds to an amplitude of 0. By combining the two binary logical inputs (Table 1), four possible input combinations are generated. Furthermore, the superposition of s_1 and s_2 results in a three-level aperiodic square wave with possible amplitudes of 0, 0.3, or 0.6 (see Table 1). The logical output of the chaos-driven FHN neuron in response to the external current I is defined according to its dynamical state. A resting state is encoded as 0, while an excited state is represented as 1. The detection of spiking activity is based on upward crossings of the zero threshold by the variable x. This encoding strategy enables fundamental logic operations such as AND and OR gates. A logical operation is deemed successful for a given gate if the following criterion is satisfied.

Table 1. The truth tables corresponding to AND and OR logic operations implemented through the FHN neuron. The neuron transitions to an excited state when an upward zero-crossing occurs in either variable x, otherwise it maintains its resting state.

Values		Logic input sets	States of neuron		Logic outputs	
(s_1,s_2)	s_1+s_2		AND	OR	AND	OR
(0,0)	0	(0,0)	resting	resting	0	0
(0,0.3)/(0.3,0)	0.3	(0,1)/(1,0)	resting	excited	0	1
(0.3,0.3)	0.6	(1,1)/(1,0)	excited	excited	1	1

Subsequently, the success probability P is defined to quantitatively evaluate the reliability of the logic operations in the proposed system, and the formula for calculating P is as follows:

$$P = \frac{N_{\mathrm{s}}}{N_{\mathrm{t}}}, \tag{7}$$

where N_{s} is the number of successful runs, and N_{t} is the total number of runs. For each combination of logic inputs, a simulation trial is considered successful if the system output consistently matches the expected values specified in the truth table throughout the run. Due to inherent transmission delays in the system, transient failures occurring within the initial 10% of the simulation period are excluded from the evaluation of the success probability P. To ensure statistical reliability, the total number of trials is set to 1000, with each trial spanning a duration of 10000 time units. It should be noted that control experiments using larger trial counts, longer simulation durations, and smaller time steps produced no significant differences in the outcomes.

3. Results and discussion

We employed the Euler method with a fixed time step of $\Delta t = 0.001$ time units to numerically integrate the dynamical Eqs. (5) and (6). The initial values of all variables were randomly assigned within appropriate ranges. It should be noted that control simulations confirmed that neither using a smaller time step nor varying the initial conditions led to significant differences in the results. In the numerical simulations, the values of the other parameters are set as follows: $\varepsilon = 0.01$, $k = 0.01$, $k_1 = 0.5$, $k_2 = 1.0$, $V_{\mathrm{syn1}} = 1.5$, $\sigma_1 = 8$, $\theta_1 = -0.3$, $V_{\mathrm{syn2}} = 2.0$, $\sigma_2 = 10$, and $\theta_2 = -0.25$.

3.1. Multi-scale autapse-induced logical resonance for AND operation

To explore the mechanisms by which chaotic driving enables the improved neuron model to perform logic computations, we first analyzed the fundamental dynamical properties of the system and subsequently tested its practical performance in logic computing tasks. The results are shown in Fig. 1.

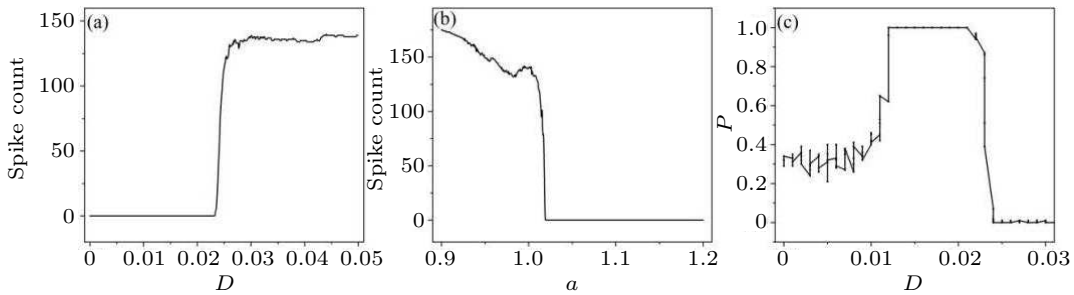


Fig. 1. Spike count with parameter scanning (a) $a = 1.05$, $I = 0.3$. (b) $D = 0.015$, $I = 0.3$. The AND logic success rate (c) $a = 1.05$.

The results in Fig. 1 indicate that the system can exhibit stable periodic oscillations within an appropriate parameter range. We analyzed the computational performance of the system in implementing the AND logic gate and plotted the success rate as a function of the chaotic driving intensity D. The findings are consistent with the dynamical analysis of the underlying system: moderate chaos enhances computational capability and adaptability, whereas excessive chaos undermines computational reliability. Specifically, the success rate of logic computation reaches its maximum within the intermediate range of chaotic driving intensity. For this purpose, external input signals S_1 and S_2, along with their linear superposition, are constructed as system stimuli, and the membrane potential variable x is sampled under varying synaptic strength parameters. As shown in Fig. 2, the time-series responses of the system are presented for three typical synaptic time conditions. It is observed that, within a specific parameter range, the system exhibits synergistic behavior in nonlinear dynamics.

Figure 2 primarily examines the regulatory effect of multi-scale autaptic connections on AND logical resonance under varying synaptic time constants τ_2. When only a single autapse is present, no significant correlation is observed between neuronal firing activity and the input signals. Under fixed chaotic driving intensity and synaptic current strength, the system exhibits significant dynamical state transitions by adjusting the parameter τ_2. When τ_2 is further increased to 0.08 ms, the prolonged duration of the synaptic current leads to excitatory saturation. When τ_2 is set to 0.4 ms, the system attains an optimal dynamical regime characterized by regular full-amplitude action potentials. The membrane potential demonstrates pronounced synchronization with the chaotic input signal, providing clear evidence of chaotic resonance. When $\tau_2 = 0.6$ ms, the synaptic current decays too rapidly, and the membrane potential exhibits oscillatory behavior that does not synchronize with the input signal, thereby failing to achieve effective logical resonance. Although the amplitude of the membrane potential response increases, the firing pattern becomes irregular, exhibiting nonlinear phenomena such as complex spikes and plateau phases. These results demonstrate that the synaptic time constant τ_2 plays a key regulatory role in multi-scale neural computation, and its optimal value can maximize signal synchronization and information transmission efficiency under chaotic driving. To determine the optimal parameter range and systematically evaluate the reliability of logical operations, the variation of the success probability with respect to autaptic time delays is investigated in this study, and the corresponding results are presented in Fig. 3.

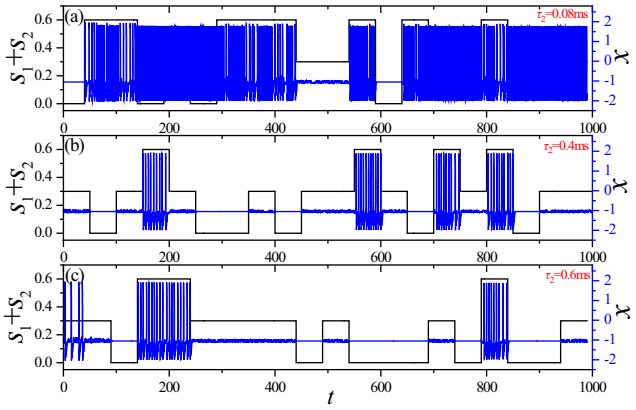


Fig. 2. Firing time series of the FHN neuron model under chaotic driving with different synaptic strengths. Black: input signal $s_1 + s_2$; blue: membrane potential. The chaotic driving intensity is $D = 0.015$, with $\tau_1 = 2$ ms, $I_{ch1} = 0.14$, and $I_{ch2} = 1.3$. Panels (a)–(c) correspond to $\tau_2 = 0.08$ ms, $\tau_2 = 0.4$ ms, and $\tau_2 = 0.6$ ms, respectively.

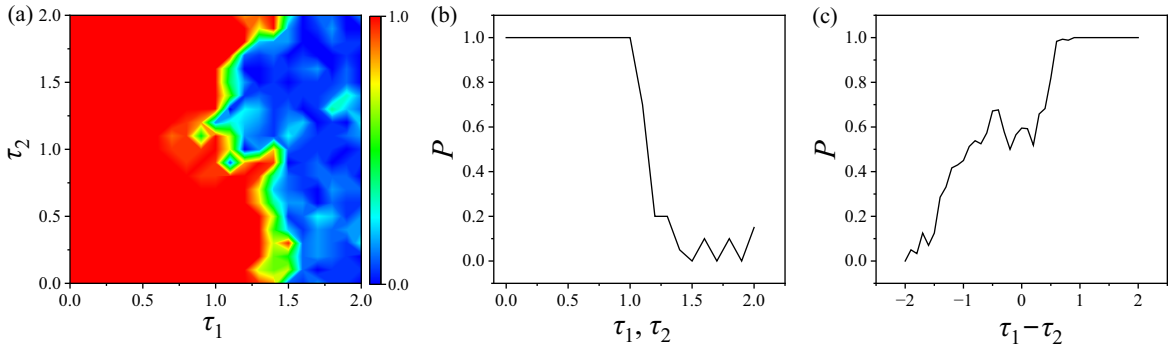


Fig. 3. Parameter dependence of AND logic performance in chaotic neuron circuits. (a) Performance landscape as a function of synaptic delays. (b) Success rate along the symmetric delay line. (c) Success rate versus delay asymmetry. The chaotic driving intensity is $D = 0.015$, $I_{ch1} = 0.14$, and $I_{ch2} = 0.3$.

The decisive influence of synaptic delay symmetry on the logical computing capability of neuronal systems is systematically revealed in Fig. 3. By scanning the delay parameter space of multi-scale autapses, a non-uniform performance distribution is observed in the success rate of AND logic operations, where specific delay combinations yield success rates exceeding 80%, thereby forming highly efficient and usable parameter regions. The trend of the success rate along the diagonal of Fig. 3(a) as a function of symmetric delay is displayed in Fig. 3(b). Notably, a broad high-performance plateau is identified near symmetric delay configurations, indicating that a balanced system design possesses enhanced

robustness. Meanwhile, the peak phenomenon presented in Fig. 3(c) suggests that computational performance may be further improved through moderate delay asymmetry. These results confirm that synaptic delay can serve as an important tunable computational parameter. To test the universality of the delay symmetry effect, the strength combinations of the multiscale autapses were systematically varied, and the results are shown in Fig. 4.

The results in Fig. 4 demonstrate that the design of neuromorphic AND gates follows a dual principle of synergistic optimization between delay and strength. On one hand, delay asymmetry serves as a key topological constraint for achieving high success rates. This conclusion remains robust across a wide range of strength parameters, indicating that temporal alignment exerts a universal influence on logical computation. On the other hand, the strength ratio regulates the morphological evolution of the performance landscape. When the strengths of the dual synapses are symmetric, the high-performance region exhibits a symmetric distribution along the diagonal of the parameter space. Under asymmetric strength conditions, however, the system forms an expanded optimal region through shifts in the delay direction, revealing an adaptive mechanism whereby delay parameters can dynamically compensate for strength imbalance. Overall, the optimization of neuromorphic logic gates relies not only on the independent adjustment of single parameters but also, critically, on the coupled design of temporal and strength dimensions. Therefore, to quantitatively characterize this coupling effect, the optimal delay difference was extracted from each subplot in Fig. 4, with the results presented in Fig. 5.

The results in Fig. 5 reveal the underlying mechanism of delay–strength coupling. In systems with symmetric synaptic strengths, the curve of success rate versus delay difference exhibits an approximately symmetric distribution centered at zero, indicating that positive and negative delay shifts produce nearly equivalent effects on system performance. Conversely, in systems with asymmetric synaptic strengths, a significant positive correlation is observed between success rate and delay difference. Specifically, when the delay of the stronger synapse exceeds that of the weaker synapse, the system can more effectively balance input disparities through temporal compensation, thereby achieving higher computational success rates. It is noteworthy that even under the ideally symmetric condition of a zero delay difference, the system success rate still fails to reach 1. A zero delay difference only ensures temporal alignment between the two input pathways but does not fully eliminate errors introduced by strength mismatch, noise interference, or model nonlinearities. This implies that the reliability of logical computation is further constrained by multiple factors, including intrinsic neuronal dynamical fluctuations and synaptic integration efficiency. To investigate the independent influence and regulatory boundaries of single synaptic parameters on logic gate performance, we calculated the performance response of one synapse across an extended parameter space, with the results presented in Fig. 6.

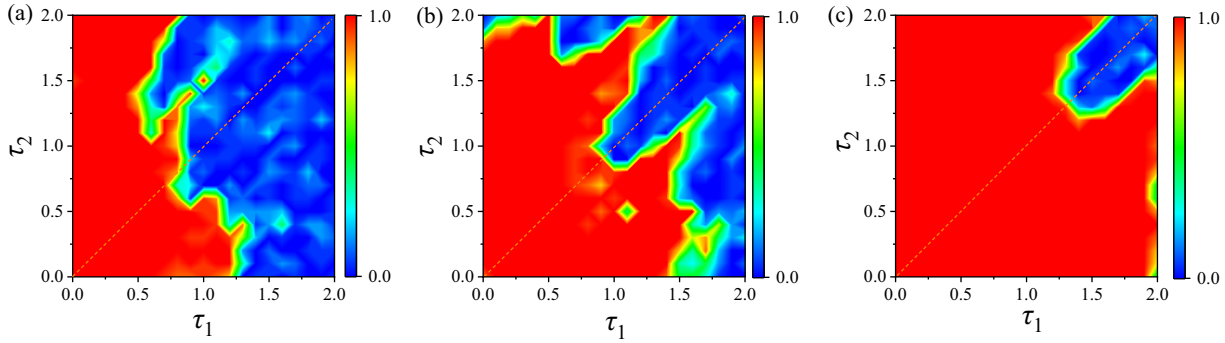


Fig. 4. Success rate landscapes for different synaptic strength pairs with $D = 0.015$. (a) $(I_{ch1}, I_{ch2}) = (0.3, 0.3)$; (b) $(I_{ch1}, I_{ch2}) = (0.14, 0.14)$; (c) $(I_{ch1}, I_{ch2}) = (0.2, 0.5)$.

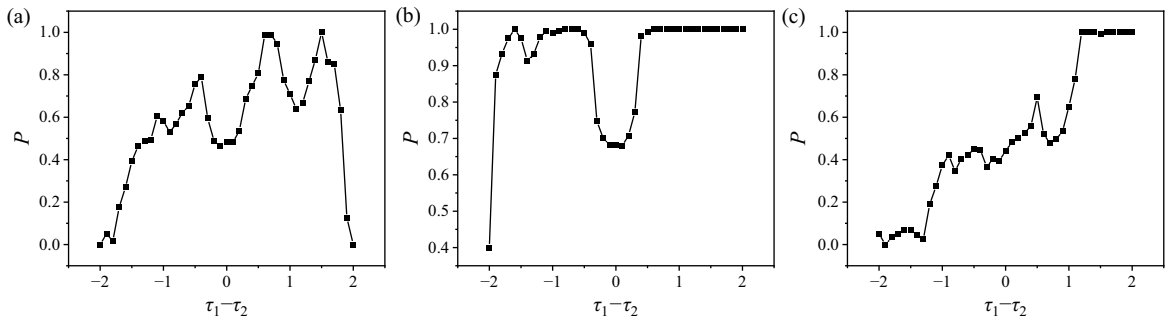


Fig. 5. Success rate versus delay asymmetry with $D = 0.015$. (a) $(I_{ch1}, I_{ch2}) = (0.3, 0.3)$; (b) $(I_{ch1}, I_{ch2}) = (0.14, 0.14)$; (c) $(I_{ch1}, I_{ch2}) = (0.2, 0.5)$.

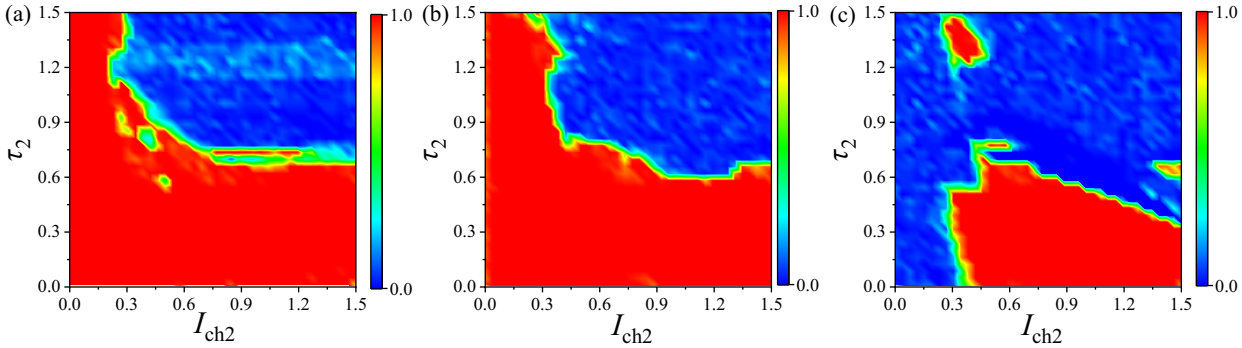


Fig. 6. Success rate landscapes for different synaptic strength pairs with $D = 0.015$. (a) $(I_{ch2}, \tau_2) = (0.14, 1)$; (b) $(I_{ch2}, \tau_2) = (0.14, 2)$; (c) $(I_{ch2}, \tau_2) = (0.3, 2)$.

Figure 6 shows that the parameter region achieving successful AND logic operations is concentrated in the area where both synaptic strength I_{ch2} and delay time τ_2 are relatively low. This outcome reveals a fundamental trade-off between synaptic strength and dynamical speed in neuromorphic logic gates. A lower I_{ch2} helps avoid over-driving the neuron and maintains response linearity, while a shorter τ_2 preserves the temporal precision of input signals, ensuring that dual pulses can effectively synchronize within a limited time window. Conversely, when both I_{ch2} and τ_2 are increased simultaneously, the combined effect of strong sustained current and slow decay drives the neuron into a state of sustained excitation or chaos. This blurs the temporal structure of input pulses and ultimately disrupts the synchronous detection mechanism required for AND operations.

3.2. Multi-scale autapse-induced logical resonance for OR operation

The results in Fig. 7 show that the delay time has a non-monotonic effect on the system performance; that is, there exists an optimal delay time value that maximizes the range of the synaptic strength window for reliable logic operation. Specifically, across all possible input combinations, the system consistently and reliably produces responses that conform to the OR logic rule, confirming the operational reliability of this logical computation. When the delay time is either too short or too long, the system's response to the input signals S_1 and S_2 deviates from the expected logical mapping, resulting in a failure to perform the intended logical operation. These findings indicate that within the multi-scale autaptic structure, there exists an optimal range of delay times within which the system can achieve the desired logical function robustly.

Furthermore, the variation of the success probability P with synaptic strength and delay time is shown in Fig. 8. A typical pattern structure can be clearly observed by systematically adjusting the autaptic coupling strength and delay time. At lower synaptic strengths, multiple logical resonances emerge. Specifically, as the delay time increases, the success rate curve exhibits multiple distinct peaks, each reaching the maximum value of 1. As the synaptic strength increases, this multiple resonance behavior gradually disappears. Nevertheless, within a certain range of delay time, the system can still exhibit high-performance logical resonance. The preceding parameter sweeps reveal the existence of high-performance regions, yet their underlying physical essence requires interpretation from the perspective of nonlinear dynamics. For this purpose, we plot the phase plane trajectories of the system under typical scenarios, as shown in Fig. 9.

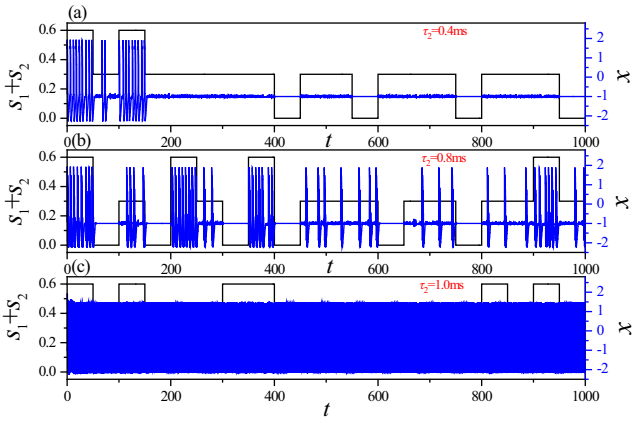


Fig. 7. Firing time series of the FHN neuron model under chaotic driving with different synaptic strengths. Black: input signal $s_1 + s_2$; blue: membrane potential. The chaotic driving intensity is $D = 0.01$, with $\tau_1 = 0.5$ ms, $I_{ch1} = 0.1$, and $I_{ch2} = 0.8$. Panels (a)–(c) correspond to $\tau_2 = 0.4$ ms, $\tau_2 = 0.8$ ms, and $\tau_2 = 1.0$ ms, respectively.

As illustrated in Fig. 9, under optimal parameter combinations, the system's nullcline structure undergoes an instantaneous change only upon the arrival of the "11" input signal, causing the resting state to disappear. The trajectory is effectively pushed across a saddle-node bifurcation, transitioning to a large-amplitude limit cycle corresponding to action potential firing. After the firing event concludes, the system accurately returns to the resting state, awaiting the next effective input. Conversely, under suboptimal parameters, the system exhibits distinctly different behaviors: either the synaptic current is too weak to cross the homoclinic bifurcation, trapping the trajectory in small-amplitude oscillations, or the synaptic current is too strong, plunging the system into sustained chaotic or irregular oscillations, thereby losing synchronization with the

input signal. This analysis confirms that the realization of logical stochastic resonance is essentially achieved through the synergistic action of multi-scale autapses, which impose precise input-dependent bifurcation control on the neuron. This control transforms the opportunities provided by subthreshold chaotic fluctuations into decisive dynamical state transitions that conform to the logical rules. The multiple logical resonance peaks in Fig. 8 are the dynamic manifestation of the bifurcation mechanisms in Fig. 9. Optimal autaptic parameter combinations trigger a saddle-node bifurcation for precise spiking and form these distinct peaks. Reduced success probability between peaks results from subthreshold or chaotic oscillations. These abnormal bifurcation dynamics are all illustrated in Fig. 9.

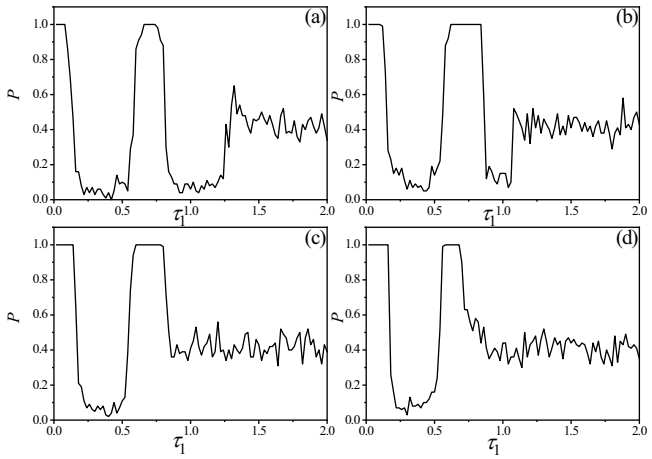


Fig. 8. The variation of success probability P with autaptic strength I_{ch2} under different delays with $D = 0.01$, $\tau_1 = 0.5$ ms, and $I_{ch1} = 0.1$. Panels (a)–(d) correspond to $I_{ch2} = 0.3$, $I_{ch2} = 0.5$, $I_{ch2} = 0.8$, and $I_{ch2} = 1.0$, respectively.

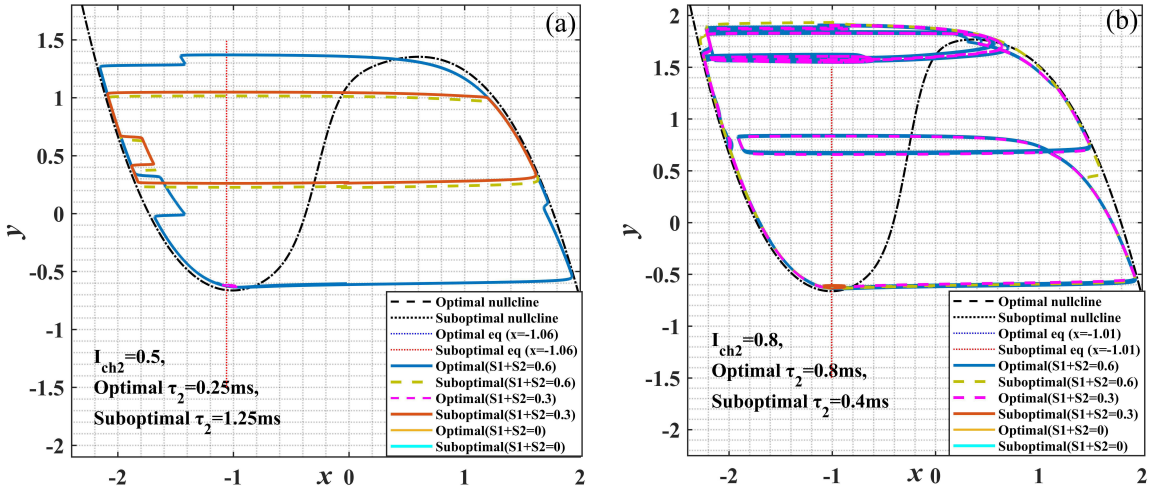


Fig. 9. Phase-plane analysis of system dynamics for logical operations. Phase trajectories for (a) AND and (b) OR operations under their respective optimal and suboptimal autaptic parameters.

4. Conclusion

This study has established that multi-scale autaptic feedback can effectively induce and optimize logical stochastic resonance in a chaos-driven neuron. Through systematic numerical investigation, we demonstrated the reliable implementation of AND and OR logic gates within a single neuron model incorporating memristive electromagnetic induction. The key advance lies in the identification of a synergistic design principle where autaptic delay and strength parameters cooperate to define high-performance operational regimes. Specifically, we found that an intentional asymmetry in synaptic delays can compensate for imbalances in connection strengths, thereby expanding the robustness window for logical computation. At lower coupling strengths, the system exhibits multiple logical resonance peaks as a function of delay time, revealing a rich dynamical landscape available for fine-tuning. Phase-plane analysis confirmed that successful logic operations correspond to precise, input-triggered bifurcations between resting and spiking states. These results provide both a deeper understanding of how biological neurons may leverage multi-scale feedback for computation and a practical co-design framework for engineering tunable neuromorphic elements based on nonlinear dynamics and memristive devices. Furthermore, the proposed framework can be extended to achieve more complex logic operations. Nonlinear logic functions such as XOR can be implemented by further adjusting the threshold parameter, autaptic strength, and time delay, or by using two neurons coupled via chemical synapses.[48,49] In future work, we will explore the realization of more universal logic gates including XOR and NAND, which will help build a complete library of neuromorphic logic units and support the development of reconfigurable and low-power neuromorphic hardware.

Acknowledgments

Project supported by the Key R&D Program of Shandong Province, China (Grant No. 2025CXPT087) and the National Natural Science Foundation of China (Grant No. 12402061).

References

[1] Roy K, Jaiswal A and Panda P 2019 *Nature* **575** 607
[2] Wysoski S G, Benuskova L and Kasabov N 2010 *Neural Networks* **23** 819
[3] Patino-Saucedo A, Rostro-Gonzalez H, Serrano-Gotarredona T and Linares-Barranco B 2020 *Neural Networks* **121** 319
[4] Renart A, De La Rocha J, Bartho P, Hollender L, Parga N, Reyes A and Harris K D 2010 *Science* **327** 587
[5] Wu Y, Deng L, Li G, Zhu J and Shi L 2018 *Front. Neurosci.* **12** 331
[6] Lu S, Dai Z, Liu Y, Liu G, Yang H and Wang F 2019 *Chin. J. Phys.* **58** 179
[7] Yang H, Yao Y and Ren J 2022 *Chin. J. Phys.* **77** 124
[8] Yao Y and Yao C 2023 *Nonlinear Dyn.* **111** 4807
[9] Huang H, Ren R and Deng K 2022 *Chin. J. Phys.* **77** 269
[10] Brown D, Feng J and Feerick S 1999 *Phys. Rev. Lett.* **82** 4731
[11] Xu Q, Chen X, Chen B, Wu H, Li Z and Bao H 2023 *Nonlinear Dyn.* **111** 8737
[12] Murali K, Sinha S, Ditto W L and Bulsara A R 2009 *Phys. Rev. Lett.* **102** 104101
[13] Wu F, Guo Y, Ma J and Jin W 2023 *Appl. Math. Comput.* **455** 128131
[14] Zhou P, Xu Y and Ma J 2023 *Physica A* **620** 128746
[15] Wang Z, Qiao Z, Zhou L and Zhang L 2017 *Chin. J. Phys.* **55** 252
[16] Yu D, Yang L, Zhan X, Fu Z and Jia Y 2023 *Nonlinear Dyn.* **111** 6757
[17] Wang X, Yu D, Li T and Jia Y 2023 *Physica A* **630** 129247
[18] Wang X, Jia K and Ge M 2025 *Chin. J. Phys.* **97** 1355
[19] Njitacke Z T, Takembo C N, Koumetio B N and Awrejcewicz J 2022 *Nonlinear Dyn.* **110** 2793
[20] Ma J, Song X, Tang J and Wang C 2015 *Neurocomputing* **167** 378
[21] Wang H, Ma J, Chen Y and Chen Y 2014 *Commun. Nonlinear Sci. Numer. Simul.* **19** 3242
[22] Yao C, He Z, Nakano T, Qian Y and Shuai J 2019 *Nonlinear Dyn.* **97** 1425
[23] Yilmaz E, Baysal V, Perc M and Ozer M 2016 *Sci. China Technol. Sci.* **59** 364
[24] Baysal V, Erkan E and Yilmaz E 2021 *Philos. Trans. R. Soc. A* **379** 20200237
[25] Zhao Z, Li L and Gu H 2020 *Commun. Nonlinear Sci. Numer. Simul.* **85** 105250
[26] Markovic D, Mizrahi A, Querlioz D and Grollier J 2020 *Nat. Rev. Phys.* **2** 499
[27] Xu K and Wang Z 2023 *Neural Comput. Appl.* **35** 8785
[28] Zhou P, Xu Y and Ma J 2023 *Physica A* **620** 128746
[29] Guo Y, Wang C and Ma J 2025 *Phys. Lett. A* **529** 130069
[30] Sun G, Xu Y, Jin W and Ren G 2023 *Physica A* **625** 129003
[31] Guo Y, Song X and Ma J 2025 *Nonlinear Dyn.* **113** 1605
[32] Ma J and Guo Y 2024 *Chaos Solitons Fractals* **183** 114925
[33] Xu Y and Qin H 2024 *Chin. J. Phys.* **92** 1384
[34] Sun G and Xu Y 2025 *Commun. Theor. Phys.* **77** 115001
[35] Ge M, Jia K, Wang X, Liu Y and Jiang Y 2025 *Nonlinear Dyn.* **113** 26671
[36] Tuci E, Massera G and Nolfi S 2010 *IEEE Trans. Evol. Comput.* **14** 885
[37] Ma J 2025 *Nonlinear Dyn.* **113** 25365
[38] Li X and Xu Y 2024 *Nonlinear Dyn.* **112** 2253
[39] Jia J, Xie Y, Wang C and Ma J 2024 *Phys. Scr.* **99** 115030
[40] Xu Y and Li X 2025 *AIMS Math.* **10** 10976
[41] Wang B, Lv M, Zhang X and Ma J 2024 *Phys. Scr.* **99** 055225
[42] Mbeunga N K, Nana B and Woafo P 2021 *Chaos Solitons Fractals* **153** 111484
[43] Ngongiah I K, Balamurali R, Kuiate G F, *et al.* 2023 *Phys. Scr.* **98** 045221
[44] Pikovsky A S and Kurths J 1997 *Phys. Rev. Lett.* **78** 775
[45] Tabor M and Weiss J 1981 *Phys. Rev. A* **24** 2157
[46] Li Y, Schmid G, Haenggi P and Schimansky-Geier L 2010 *Phys. Rev. E* **82** 061907
[47] Belykh I, De Lange E and Hasler M 2005 *Phys. Rev. Lett.* **94** 188101
[48] Zhang H, Xu Y, Xu W and Li X 2012 *Chaos* **22** 043130
[49] Storni R, Ando H, Aihara K, Murali K and Sinha S 2012 *Phys. Lett. A* **376** 930